

LA-UR-01-5654

Approved for public release;
distribution is unlimited.

Title: **The Tagish Lake Meteorite Fall : Interpretation of
Fireball Physical Characteristics**

Author(s): P. Brown, D. O. ReVelle and A. R. Hildebrand

Submitted to:

<http://lib-www.lanl.gov/cgi-bin/getfile?00796852.pdf>

Los Alamos National Laboratory, an affirmative action/equal opportunity employer, is operated by the University of California for the U.S. Department of Energy under contract W-7405-ENG-36. By acceptance of this article, the publisher recognizes that the U.S. Government retains a nonexclusive, royalty-free license to publish or reproduce the published form of this contribution, or to allow others to do so, for U.S. Government purposes. Los Alamos National Laboratory requests that the publisher identify this article as work performed under the auspices of the U.S. Department of Energy. Los Alamos National Laboratory strongly supports academic freedom and a researcher's right to publish; as an institution, however, the Laboratory does not endorse the viewpoint of a publication or guarantee its technical correctness.

THE TAGISH LAKE METEORITE FALL : INTERPRETATION OF FIREBALL PHYSICAL CHARACTERISTICS

P.Brown¹, D.O. ReVelle¹, and A.R. Hildebrand²

¹Los Alamos National Laboratory, MS J577, Los Alamos, NM 87545 USA email:pbrown@lanl.gov

²Department of Geology and Geophysics, University of Calgary, Calgary, Alberta, CANADA : hildebra@geo.ucalgary.ca

ABSTRACT

We have analyzed available instrumental and eyewitness records associated with the fireball leading to the fall of the Tagish Lake meteorite. Initial chemical and physical studies of this carbonaceous chondrite have shown it to be unique. It is one of the most primitive meteorites yet recovered and extremely friable. By determining the original bodies trajectory, velocity and physical breakup in the atmosphere we can characterise the fireball as intermediate between Type II and Type IIIa, following the classification of Ceplecha et al. (1998). Modelling of the object suggests an initial porosity for the pre-atmospheric body in the range 40-60%. The initial fragmentation occurred under less than 0.3 MPa dynamic pressure. Determination of Tagish Lake's orbit suggests a nominal linkage to parent bodies in the main asteroid belt, though association with short-period comets cannot be strictly excluded. It is suggested that Tagish Lake represents an intermediate object between chondritic asteroids and cometary bodies and our results are consistent with a linkage to D-class asteroids based on results from reflectance-spectra work.

1. INTRODUCTION

The Tagish Lake meteorite fell on January 18, 2000 at 16:43:43 UT (08:43:43 local time). The fireball accompanying the meteorite fall was widely observed over the Yukon Territory and British Columbia in Canada as well as parts of Alaska. The fireball was of unusually long duration; many observers reported it to be visible for 15-20 seconds. That the duration of the event was significant is verified by a security video camera record which shows increased illumination of the local terrain for just over ten seconds associated with the fireball. The peak brightness of the fireball was enough to illuminate the still dark terrain to near daylight conditions for observers nearest the endpoint. The final portion of the fireball trajectory was dominated by one short major burst followed by a more extended terminal disintegration. Reports from eyewitnesses invariably de-

scribed these two major detonations as primary features of the event. Substantial delayed sounds were registered by observers at distances of up to 200 km from the fireball trajectory. In addition to these delayed sounds, several reports of electrophonic sounds (cf. Keay et al., 1980) were also documented. Particularly notable amongst the documented records are several reports of unusual smells being detected at nearly the same time to slightly following the fireball proper. Observers uniformly reported these smells to be of a fowl metallic, chemical odour.

In addition to these eyewitness records, a total of five video records and 24 still photographs of the associated dust cloud were made by casual observers. Figure 1 shows an example of the still photos taken shortly after the fireball. In addition to these data, sensors on US Department of Defence satellites detected the event in the infrared (providing positional information) and at optical wavelengths (defining the light curve). The space-based records include a fortuitous image of the dust-cloud made by the Defence Meteorological Satellite Program F-13 satellite which scanned the area near the endpoint of the fireball only two minutes after the event. Figure 2 shows this space-based record of the fireball dust cloud.

The airwave signal from the fireball was recorded on three local seismic stations, Whitehorse (WHY), Haines Junction (HYT) and Dease Lake (DLBC). These show both direct air-coupled rayleigh wave arrivals as well as seismically coupled body waves due to the airblast.

Of greatest value for the interpretation of the fireball data is the recovery of meteorites from the ice surface of the Taku Arm of Tagish Lake over the interval January - May, 2000 (cf. Brown et al., 2000). In total some 410 individual fragments from the fireball were located and more than 200 samples recovered for later analysis, totalling approximately 5 kg of material. Based on the available fall data, the physical characteristics of the recovered samples and modelling of the event here we attempt to reconstruct the pre-atmospheric orbit and physical character of the original Tagish Lake meteorite body.

2. CALCULATION OF THE FIREBALL TRAJECTORY, VELOCITY, INITIAL MASS AND ORBIT

2.1. Velocity and Atmospheric path



Figure 1. Dust cloud remaining after the passage of the Tagish lake fireball. This image was still-framed captured from video of the dust cloud shot by Doug Davidge from Whitehorse, Yukon Territory several minutes after the fireball. The recording was made using a Sony TRV75 Hi-8 camcorder equipped with extended infrared response. The bright portion of the trail near the lower part of the image represents that segment of the trail where the sun is within a few degrees of rising above the local horizon and hence appears most heavily illuminated.

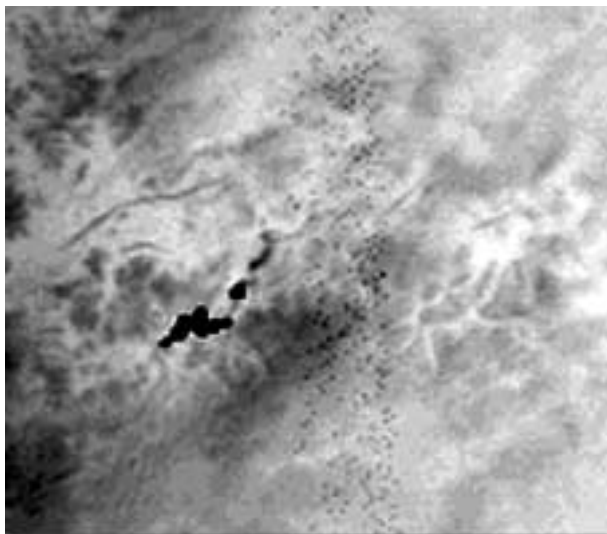


Figure 2. Visible light detection of the fireball dust cloud from space. This image was captured by the Defence Meteorological Satellite Program F-13 satellite. The satellite scanned through the dust trail (dark cloud left of center) approximately two minutes after the passage of the fireball. The image has been inverted for clarity.

To compute the fireball trajectory we first make use of existing eyewitness data. In total over 90 persons were interviewed and measurements made of the observed path of the fireball in the Yukon and British Columbia. These data, however, are widely discordant and do not provide a good estimate for the overall trajectory. In particular, the slope of the fireball path in the atmosphere is particularly uncertain from these data. However, sufficient visual observations exist close to either side of the ground track to strictly constrain the fireball apparent radiant azimuth to be in the range $327^\circ \leq \phi \leq 334^\circ$. Using the best eyewitness data and the least-squares solution method of Borovicka (1990), the formal trajectory solution (with formal error) is given in Table 1. Note that this solution does not make use of the observers proximate to the ground track as these were observations of the dust cloud only. The relatively flat trajectory of the fireball is qualitatively reflected in numerous visual observers who (incorrectly) reported following the fireball to the southern horizon. The eyewitness solution should be treated very cautiously as the real errors are much larger than the formal error margins shown. Indeed, solutions with entry values from near zero to 25° and azimuths from 320° to nearly 350° may be accommodated with different (subjectively chosen) subsets of the eyewitness reports using the least-squares technique.

More accurate determination of the trajectory is possible by making use of the photographs and video of the associated dust cloud. In particular, of all the instrumental records of the dust cloud, three were made very shortly after the fireball, had good positional references in the fields of view and were well separated spatially so as to provide a good path solution. An example of one of these is given in Figure 3. These observations consist of a video recordings made from Whitehorse (60.718°N , 135.054°W) (Wheeler) beginning about 15 seconds after the fireball, a still photo of the dust cloud from 60.367°N , 134.089°W approximately 120 seconds after the event (Ford) and finally a still digital photo of the dust cloud from Atlin, British Columbia (59.572°N , 133.703°W) taken 90 seconds after the fireball (Lemke).

To better define the original trajectory, the video record from Whitehorse was used to define the upper wind motions. As can be seen from Figure ??, by following the dust cloud over a period of several minutes, the local wind vectors are well defined at different points along the trail. To define the best fits for each observation, the same points on each trail were identified and the approximate wind vectors were inverted to redefine the original fireball trail – this iterative process was stopped when the modelled dust



Figure 3. Dust cloud photo taken from Atlin, British Columbia by Ewald Lemke.

trails became nearest to linear at each site. Using the resulting apparent trajectories plus the original dust cloud measurements, a best-fit trajectory was determined as shown in Table 1.

To compute the velocity, common features in the optical light curve were compared with the infrared satellite measurements. From this comparison a mean velocity prior to the main burst of $15.5 \pm 0.6 \text{ km s}^{-1}$ was measured. Comparison of the satellite optical light curve and measured features on the most detailed dust cloud photos (Lemke) yield a velocity of 15.7 km s^{-1} prior to the main burst and velocities approaching 9 km s^{-1} at the end of the visible light curve.

Taking the satellite derived trajectory as most accurate and an initial velocity of $15.8 \pm 0.6 \text{ km s}^{-1}$ (corrected for early deceleration of the large pre-atmospheric meteoroid as shown in the next section) the orbit solution is shown in Table 2. The orbit is similar to previously measured meteorite orbits.

2.2. Initial Mass

The most direct measure of the initial mass of the body comes from satellite records of the event. Figure 4 is the lightcurve associated with the fireball recorded by US Department of Defence satellites. Assuming the bolide radiates as a 6000K blackbody, the integrated optical light energy from the fireball is $1.1 \times 10^{12} \text{ J}$. The results of the St. Robert fireball/meteorite fall (Brown et al., 1996; Hildebrand et al., 1997) had both cosmogenic-activities from recovered meteorites (which constrained the entry mass (Herzog et al., 1997)) and satellite data available to yield an apparent luminous efficiency of 10% in the satellite pass-band for this ordinary chondrite. Using this conversion efficiency as well as the integrated optical energy and the initial velocity determined from the previous section we derive an initial mass estimate near $9 \times 10^4 \text{ kg}$. Given the unusual makeup of Tagish Lake as compared to H-chondrites, we antici-

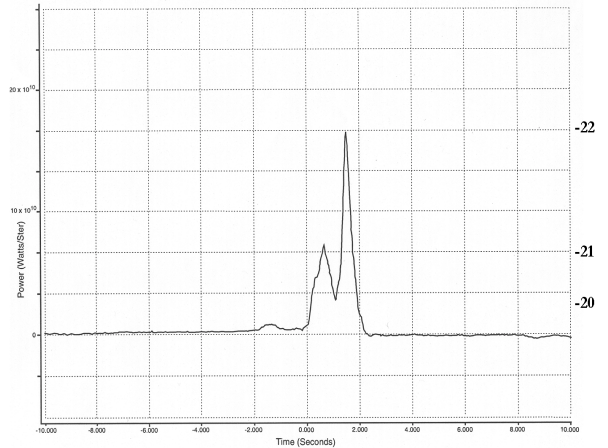


Figure 4. Optical satellite light curve. The right axis shows approximate absolute visual magnitude assuming a 6000K blackbody. Zero time is 16:43:42s UT on 18 January, 2000.

pate this efficiency will be somewhat different. Taking the widest range of physically probable efficiencies to be from 5-20%, implies probable mass ranges from $5 \times 10^4 - 1.8 \times 10^5 \text{ kg}$.

To better estimate this initial mass, we use the entry model employed to interpret the lightcurve and initial mass for the St. Robert fireball (Brown et al., 1996), namely that of the gross fragmentation model of Ceplecha et al. (1993). Here we adopt the entry angle, initial velocity, apparent heights of initial break-up and satellite observed light curve as constraints for the modelling. Our goal is to determine the initial mass, using only a constant ablation coefficient as an assumed input. We note that the light so-produced is referenced to the revision in the luminous efficiency scale computed by Ceplecha (1996) from analysis of the Lost City meteorite fall of 5.2%. We expect for such a fragile body that the value for the ablation coefficient (σ) will be larger than chondritic values and most likely in the range $0.04 - 0.20 \text{ sec}^2 \text{ km}^{-2}$. The implication of this larger σ is that the effective luminous efficiency will be higher than the chondritic value (cf. ReVelle, 1983) and our estimates extreme upper limits (within the constraints of an assumed constant ablation coefficients). Figure 5 shows the results of our application of this numerical model and treating Tagish Lake as a chondritic body. The upper limit for the initial mass derived in this way is 115 Tonnes.

To examine the effects of changing σ , particularly to (more realistic) higher values, we use the mean value for type II fireballs (which are believed to be associated with carbonaceous chondrites) as given in Ceplecha et al. (1998). Here we take $\sigma = 0.042 \text{ sec}^2 \text{ km}^{-2}$ and again fit the light curve. This produces a nominal mass estimate of 97 tonnes. Extending this to higher σ makes matching the light curve and other observed parameters effectively impossible due to the simplification of using a constant ablation coefficient. However, recognizing the intrinsically higher τ val-

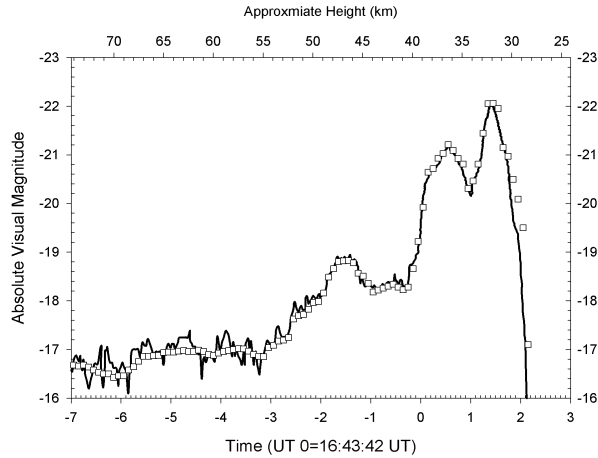


Figure 5. Optical satellite light curve (solid line) and model fit (open squares). The model fit uses parameters appropriate to an ordinary chondrite object (i.e. $\sigma=0.02 \text{ s}^2\text{km}^{-2}$ and $K=\Gamma A\rho^{-\frac{2}{3}} = 0.46$). The top axis is the approximate height, which is progressively too low (by 1-2 km) below 35 km.

ues associated with such a porous object as noted by ReVelle (1983) and the higher effective σ associated with the extensive fragmentation, we may tentatively estimate an initial mass of ≈ 65 tonnes as most probable. We estimate this measure to have an uncertainty of roughly 15 tonnes.

2.3. Seismic Data

In addition to satellite and ground-based photos/videos, the airwaves generated by the passage of the meteoroid were detected at several seismic stations. Other work has demonstrated the utility of deriving parameters for bolide trajectories from seismic data alone (cf. Qamar, 1997) when numerous stations detect the airwave. In the present case, however, only two seismic stations showed strong signals from the fireball and one other a weak probable signal. Fortunately, the entry geometry has been well-defined from satellite data.

The seismic station near Whitehorse (WHY) recorded a large impulsive (and relatively long lasting signal) beginning 208s after the main detonation recorded by the satellite (at 16:43:43 UT). Using a high-pass filter on these data (1 Hz and higher) we also note an emergent waveform beginning some 128s after the main detonation time. These phases are shown in Figure 6.

The strongest arrival is associated with the main airblast. This phase we suggest starts with the first direct arrival of the airwave from the ballistic shock, having propagated from the trajectory as a cylindrical blast wave. Rayleigh waves moving at acoustic velocities in the topmost portion of the soil near the seismic station arrive next. The earliest arrival of the airwave phase is that of an N-wave

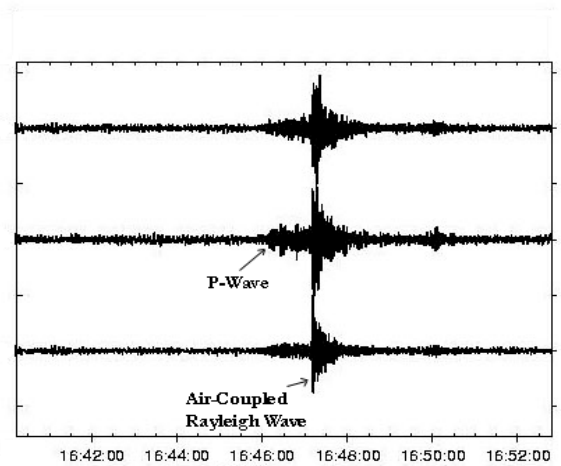


Figure 6. High-pass filtered seismic record from WHY showing P-wave and Rayleigh wave arrivals. The three components shown are (from top) the E, N and Z-components. Amplitudes are normalized within each component.

signature in the vertical component of the seismograph (showing strong downward motion), indicative of that expected of shock loading of the local terrain (cf. Kanamori et al., 1991). The large amplitude of this arrival phase is typical of seismically-coupled rayleigh waves which often are the strongest component of seismic records of airblasts due to resonant coupling with loose soil (Ewing et al. 1967).

Similarly, we expect that the P-wave signature reflects coupling near the sub-terminal point of the fireball, where the earliest portion of the blast wave first reaches the earth. Indeed, provided the amplitude of the blast is sufficient, we expect the shock to couple directly into the ground very near the locus of points directly under the trajectory where the trace velocity across the ground of the cylindrical blast wave is comparable to the local P-wave velocity (which we adopt as 6 km^{-1}). Thus the earliest P-wave signal should be from the region nearest the terminal portion of the fireball where a significant blast wave is still produced. Our final P-wave solution times and heights are relatively insensitive to values for P-wave velocity different from the above. The effect of lower P-wave speeds (which would be the expected trend in a mountainous region) will be to push the solution to slightly higher heights.

To further examine the question of the origin of these seismic waves, we have taken the fireball trajectory determined from the satellite data as being most representative of the true trajectory and modelled the expected arrival times of waves at WHY. We have used radiosonde data from WHY taken at 12 UT on Jan 18, 2000 as an input atmosphere to an altitude of 30 km and used the MSIS-E NASA atmosphere model above this height to define the acoustic velocity as a function of height. Ignoring wind corrections to this apparent sound velocity, we have computed the airwave arrivals at WHY as a function of height along the fireball path. Similarly, we compute the

arrival times for P-waves, using the previously described model of the airblast travelling to ground then the P-waves travelling to the seismic station. A graphical version of the resulting solution is shown in figure 7.

A priori, ignoring fragmentation (which produces quasi-spherical point sources along the trajectory) we expect the ballistic-weak-shock to propagate approximately normal to the fireball trajectory (cf. Revelle, 1976). As a result, this airwave should have an origin with that portion of the trajectory of the fireball passing closest to the station. In figure 7 this would be the minima in the parabolic time propagation curve. In fact, the large-amplitude acoustic arrival occurs almost 20 seconds after this point.

To determine if this discrepancy is due to our ignoring the upper winds in calculation of the sound velocity, we have numerically modelled ray arrivals to the station from along the fireball trajectory. This simulation uses the same atmosphere as described earlier, but explicitly takes into account the wind velocity and ray propagation geometry in computing ray arrival times. As the wind velocity was very high near 30km altitude (almost 70 m/s), we expect this may produce significant deviations from our nominal curves, making the sound velocity a function of propagation azimuth.

The model results for propagation from various source heights are shown in figure 7 as solid squares. The wind effects are clearly evident and account nicely for the timing difference. Where several rays reach WHY we have shown the extreme range in arrival times for a given height. The numerical results suggest that the beginning of the main seismic signal (and the largest amplitude) is indeed from the ballistic wave propagating nearly normal to the fireball path, with significant modifications from the upper wind.

The main seismic signal beginning 208s after the detonation continues for approximately 84s. This is longer than would be expected if only the portion of the trail near the specular point were contributing the airwave signal where dispersion effects which spread the acoustic signal in time are minimal. Anglin and Haddon, 1987 and Cumming, 1989 both show examples of acoustically-coupled seismic waves from bright fireballs - in both cases the signals persist for ≤ 10 seconds. In our records, there are several additional maxima during this 84 second window. While some contribution from the P-wave may be present early in the record, it is unlikely to persist for this entire interval or show such localized maxima. We note that the extended signal could be a consequence of the properties of the soil proximal to the seismograph. No simple means of determining if extended resonance effects due to local ground properties are significant; we can only indicate that these are not seen for fireball airwaves recorded by other seismic instruments at different locations.

One interpretation of this extended signal is that it

represents acoustic energy from ongoing gross fragmentation not represented in the cylindrical blast wave model and propagating in a wider suite of directions (ReVelle, 1976) to WHY. Such a model would suggest arrivals at WHY from the terminal portions of the fireball where the satellite light curve shows significant ablation and (by inference) possibly fragmentation. This is similar to the interpretations of Cumming, 1989 and Folinsbee et al. 1969 where seismic data were compared to photographically determined fireball trajectories and suggested almost all the acoustic signal was due to acoustic energy generated near the terminal portions of the trajectory. In both cases these locations significantly different than the specular points along the trajectory relative to the receiving seismic stations.

Examining figure 7 we see that the numerical ray modelling shows acoustically accessible paths from heights along the trajectory restricted to those greater than 37 km altitude. Our numerical modelling reveals that lower heights may produce acoustical signatures, but these are just inside the first acoustic shadow zone of the sound as seen from WHY and would not contribute significantly to the seismic signal. Figure 9 demonstrates this effect.

That the numerical arrival times end within 10 seconds of the cessation of the main seismic signal suggests that fragmentation along the latter portion of the path is a plausible production mechanism for the extended signal. We also note that while heights along the fireball path below 38 km will not contribute significantly to the signal, our ray modelling is a geometrical approximation which ignores scattering and diffraction effects whereby lower portions of the trajectory may contribute to some of the trailing end of the main signal.

On the basis of seismic data from WHY, we suggest that the major portion of the large scale fragmentation for the Tagish Lake fireball ended near 32 km altitude. The seismic solution for station HYT is shown in figure 8 and supports this height determination. The WHY seismic record also suggests that this fragmentation dominated the last 45-60 km (3-4 seconds of light production) of the path in agreement with the satellite light curve which shows almost 4 seconds of noticeable signal (corresponding to ≈ 60 km at the nominal initial entry velocity).

3. PHYSICAL INTERPRETATION

3.1. Meteorites

The meteorites recovered from the Tagish lake fireball have been classified as C2, ungrouped. They represent a primitive form of carbonaceous chondrite, perhaps the most primitive meteorite studied to date (cf. Brown et al., 2000). Recent studies of the reflectance spectra from powdered Tagish Lake material also suggest a linkage with D-class aster-

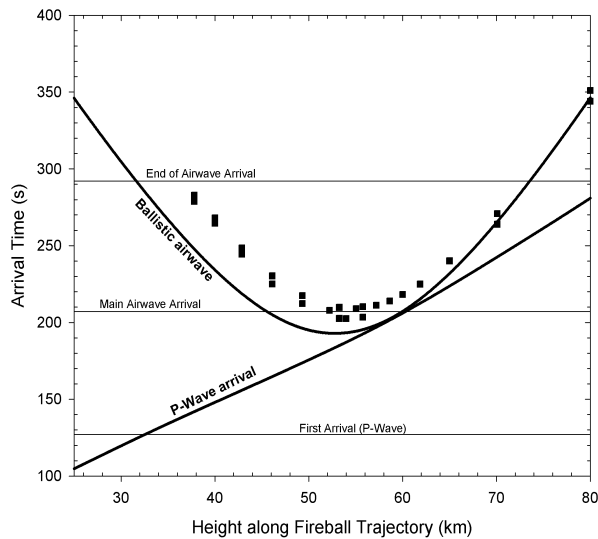


Figure 7. Seismic wave arrival times (labelled horizontal lines) and nominal air wave arrival times at WHY using a mean sound velocity as a function of height along the fireball trajectory (parabolic line). The zero time is the time of the fireball main detonation (16:43:43 UT). Also shown is the solution for P-wave arrivals. Square symbols represent numerical solutions from ray-path modelling at each height to WHY as described in the text. These model solutions show those heights at which acoustic ray paths to WHY exist - this does not imply actual acoustic signals arrive from such heights as this also depends on the source generation mechanism, i.e. ballistic cylindrical shock vs. fragmentation. All modelled travel times have been corrected for the fireball's velocity.

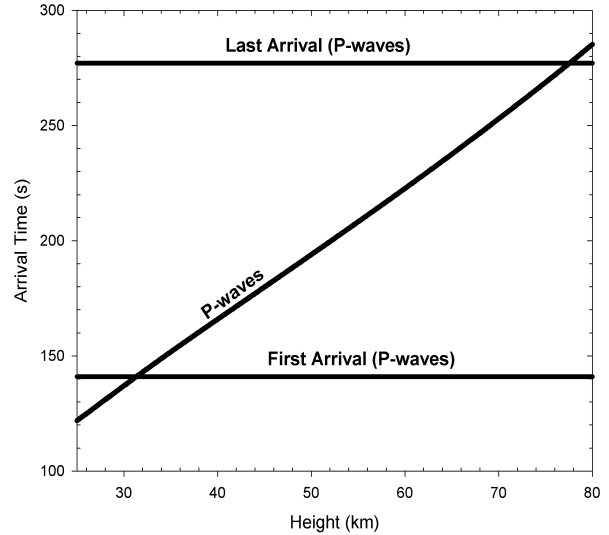


Figure 8. Seismic wave arrival times (labelled horizontal lines) at HYT using a mean sound velocity as a function of height along the fireball trajectory. The zero time is the time of the fireball main detonation (16:43:43 UT). Also shown is the solution for P-wave arrivals. All modelled travel times have been corrected for the fireball's velocity.

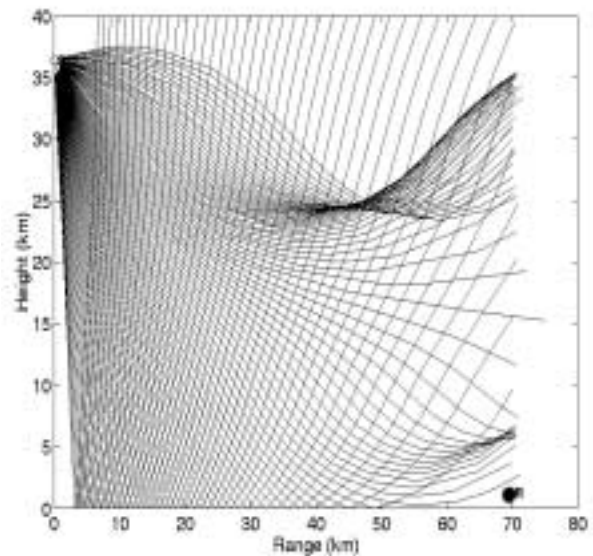


Figure 9. Acoustic ray paths from the location of the main burst to WHY (labelled as R in the lower right-hand corner of the figure). Notice the lack of rays reaching the receiver for this height.

oids (Hiroi et al., 2001). This would represent the first connection between D-class asteroids and meteoritic material. This further supports the supposition that Tagish Lake material is primitive, given the presumed supercarbonaceous origins for the D-class asteroids (cf. Bell et al., 1989).

To further examine the physical character of the original Tagish lake object, we have measured the densities and porosities of several Tagish lake specimens. The results are shown in Table 2. The porosity and bulk density for Tagish lake is among the lowest yet measured for meteorite material. Only the Orgueil CI-chondrite has been reported with comparable porosity and bulk densities, though controversy exists as to whether these low values may be due to weathering effects (cf. Corrigan et al., 1997).

We expect that the material recovered from Tagish Lake preferentially represents the strongest portions of the original brecciated body. The implication of these measurements is that the original pre-atmospheric Tagish lake meteoroid had comparable or higher porosities and lower bulk densities to those given in Table 2. This would imply probable porosities in the range of 40–60%.

3.2. The Fireball

To attempt to place the Tagish Lake fireball in the context of physical data available for other fireballs, we make use of the PE-criterion introduced by Ceplecha and McCrosky (1976). This statistical index is a proxy measure for the relative physical strength of the associated meteoroid based on the ability of the associated fireball to penetrate the atmosphere. More specifically, the PE-criterion is given by

$$PE = \log(\rho_E) - 0.42 \log(m_\infty) + 1.49 \log(V_\infty) - 1.29 \log(\cos(Z_R)) \quad (1)$$

where ρ_E is the air density at the fireball end-point, m_∞ is the initial mass, V_∞ is the initial velocity and Z_R is the zenith angle of the trajectory. Ceplecha and McCrosky (1976) suggested four basic physical groupings existed in the fireball record, from the strongest, most penetrating material (Group I) to the weakest material (Group IIIb). These groupings have been associated with (cf. Ceplecha et al., 1998), ordinary chondrites, carbonaceous chondrites, strong cometary material and weak cometary material for groups I, II, IIIa and IIIb respectively. We emphasize that the exact PE values where one group ends and another begins is somewhat uncertain as this is a purely statistical measure. From our best estimate for the initial mass of the Tagish Lake object (65 Tonnes), its initial velocity (15.8 km/s), its known zenith angle at entry (72.2°) and the last observed dust cloud "point" from the ground based data of 29 km, we arrive at a PE=-5.39. This is near the

border of the Type II and IIIa groups (which split at PE=-5.25). Given the statistical uncertainties in the broader groups, we suggest that Tagish Lake represents the low end of the strength spectrum for carbonaceous chondrites or the very highest end of the cometary strength spectrum. This is consistent with the physical evidence from the meteorites.

4. DISCUSSION AND CONCLUSIONS

From the above evidence, we suggest that Tagish Lake represents an object which physically bridges the population of cometary objects and the weakest "asteroidal" material existing in meteorite collections. The high porosity of measured fragments as well as the higher inferred porosity of the initial object all suggest a weakly structured object. That any material reached the surface for collection is almost certainly the result of the large initial mass, low entry angle (and hence lower dynamic pressures) coupled with the region of the fall. We speculate that Tagish Lake-type material landing in more temperate climates would be quickly eroded into chips and dust.

Of particular interest is the spectral connection between Tagish Lake and D-class asteroids (cf. Hiroi et al., 2001). We note that the only D-class asteroids to have accurate density determinations are Phobos and Deimos (cf. Britt and Consolmagno, 2000). Currently, the most accurate bulk densities for Phobos are $1.53 \pm 0.1 \text{ g cm}^{-3}$ and $1.34 \pm 0.83 \text{ g cm}^{-3}$ for Deimos (Smith et al., 1995). Comparison with Tagish Lake shows that the bulk densities are (within error) the same as the bulk density measurements for Tagish Lake. The high porosity of Tagish Lake samples ($\approx 40\%$) indicates that both Martian moons need not have significant macroporosity and suggests that appeals to large amounts of interior ice or a thick regolith (eg. Smith et al., 1995) to account for the low bulk density of the Martian moons may be unnecessary.

REFERENCES

- Anglin, F. M. & Haddon, R. A. W. 1987, *Nature*, 328, 607
- Bell, J. F., Davis, D. R., Hartmann, W. K., & Gaffey, M. J. 1989, *Asteroids II*, 921
- Borovicka, J. 1990, *Bulletin of the Astronomical Institutes of Czechoslovakia*, 41, 391
- Britt, D. T. & Consolmagno G. J., 2000, *Icarus*, 146, 213
- Brown, P. G. et al. 2000, *Science*, 290, 320
- Brown, P. et al. 1996, *Meteoritics and Planetary Science*, 31, 502
- Ceplecha, Z. & McCrosky, R. E. 1976, *Journal of Geophysical Research*, 81, 6257

- Ceplecha, Z. 1996, *Astronomy & Astrophysics*, 311, 329
- Ceplecha, Z., Spurny, P., Borovička, J., & Kečliková, J. 1993, *Space Science Reviews*, 279, 615
- Ceplecha, Z. ; K., Borovička, J. ;. Í., Elford, W. G., Revelle, D. O., Hawkes, R. L., Porubčan, V. ;., & Šimek, M. ; 1998, *Space Science Reviews*, 84, 327
- Corrigan, C. M., Zolensky, M. E., Dahl, J., Long, M., Weir, J., Sapp, C., & Burkett, P. J. 1997, *Meteoritics and Planetary Science*, 32, 509
- Cumming, G.L., 1989, *Canadian Journal of Earth Science*, 26, 1350
- Ewing, W.M., Jardetsky, W.S., & Press, F., *Elastic Waves in Layered Media*, McGraw-Hill, New York, 1967
- Herzog, G. F. et al. 1997, *Meteoritics & Planetary Science*, vol. 32, page A59, 32, 59
- Hildebrand, A. R. et al. 1997, *JRASC*, 91, 261
- Hiroi, T., Zolensky, M. E., & Pieters, C. M. 2001, *Lunar and Planetary Science Conference*, 32, 1776
- Kanamori, H., Anderson, D. L., Mori, J., & Heaton, T. H. 1991, *Nature*, 349, 781
- Keay, C. S. L. 1980, *Science*, 210, 11
- Qamar, A. 1995, *Seismological Research Letters*, 66, 6
- ReVelle, D.O. 1983, *Meteoritics*, 18, 386
- Revelle, D. O. 1976, *Journal of Geophysics Research*, 81, 1217
- Smith, D. E., Lemoine, F. G., & Zuber, M. T. 1995, *Geophysical Research Letters*, 22, 2171

Table 1. Trajectory solutions for the Tagish lake fireball using eyewitness data, the best three ground-instrumental records and satellite records. Shown is the apparent azimuth(ϕ) and altitude(θ) of the apparent radiant; the longitude (λ) and latitude (δ) of the main burst and the estimated height of the main burst

Solution	ϕ	θ	Main Burst (λ, δ)	Height of main burst (km)
Eyewitness	$319 \pm 2.6^\circ$	$9.1 \pm 3.0^\circ$	$134.630 \pm 0.18^\circ, 59.99 \pm 0.11^\circ$	31.4 ± 2.7
Instrumental	$330.7 \pm 2.4^\circ$	$14.5 \pm 1.6^\circ$	$134.645^\circ, 60.040^\circ$	37.6 ± 1.7
Satellite	330.7°	17.8°	$134.6^\circ, 60.02^\circ$	35

Table 2. Orbit for the Tagish Lake fireball using the satellite recorded solution. All angular coordinates are $J2000.0$

V_∞	$15.8 \pm 0.6 \text{ kms}^{-1}$
α_G	$89.9 \pm 2.2^\circ$
δ_G	$29.8 \pm 2.4^\circ$
a	$2.0 \pm 0.2 \text{ A.U.}$
e	0.56 ± 0.04
q	$0.885 \pm 0.010 \text{ A.U.}$
ω	$223.9 \pm 2.2^\circ$
Ω	$297.901 \pm 0.001^\circ$
i	$2.0 \pm 0.9^\circ$
Q	$3.2 \pm 0.4 \text{ A.U.}$

Table 3. Physical data for densities and porosities for two Tagish Lake specimens. $M(g)$ is the measured mass in grams while mineral ρ is the mineral density of the specimen (gcm^{-3}) as measured by a helium pycnometer. The bulk ρ is the bulk density computed from the mass and volume (measured using fine glass beads). The porosity is a measure of the void space in the object and is computed from the mineral density and mass. The first two columns are data for the measured specimens for Tagish Lake. Data for Orgueil (CI chondrite) and other meteorite class averages are taken from Britt and Consolmagno (2000).

Sample	$M(g)$	Mineral ρ	Bulk ρ	Porosity (%)
Tagish Lake (RB)	30.44	2.74	1.65 ± 0.15	40 ± 10
Tagish Lake (ET-06)	77.19	2.56	1.61 ± 0.10	37 ± 6
Orgueil	47.2	2.43	1.58 ± 0.03	35 ± 7
H-Chon (Av.)	-	3.70	3.46	5
CM-Chon (Av.)	-	2.71	2.21	12